

Charge and magnetic ordering in the electron-doped magnetoresistive materials $\text{CaMnO}_{3-\delta}$ ($\delta=0.06,0.11$)

C. R. Wiebe and J. E. Greedan

The Brockhouse Institute for Materials Research, McMaster University, Hamilton, Ontario, Canada L8S 4M1

J. S. Gardner

The Neutron Program for Materials Research, NRC, Chalk River Labs, Chalk River, Ontario, Canada K0J 1J0

Z. Zeng and M. Greenblatt

Chemistry Department, Rutgers University, Piscataway, New Jersey 08854-8087

(Received 9 August 2000; revised manuscript received 1 February 2001; published 24 July 2001)

The magnetoresistive “electron”-doped materials $\text{CaMnO}_{3-\delta}$ ($\delta=0.06,0.11$) have been investigated using powder neutron diffraction. The two materials are n -type semiconductors which exhibit antiferromagnetic ordering at $T_N \sim 125$ K, but they have different magnetic structures. The $\text{CaMnO}_{2.94}$ sample orders in a simple G -type antiferromagnetic structure, which is also observed in CaMnO_3 . The $\text{CaMnO}_{2.89}$ sample, on the other hand, exhibits two magnetic features: the G -type reflections as noted above, and a set of reflections that can be indexed on a $k=(0,0,\frac{1}{4})$ ordering wave vector. A model for the magnetic structure is proposed which involves $\text{Mn}^{3+}/\text{Mn}^{4+}$ charge ordering concomitant with the magnetic ordering. The presence of a set of weak, temperature independent structural reflections which can also be indexed on a $k=(0,0,\frac{1}{4})$ supercell suggests an oxygen vacancy ordering which may play a role in the charge ordering.

DOI: 10.1103/PhysRevB.64.064421

PACS number(s): 75.25.+z, 75.30.-m, 75.50.-y

INTRODUCTION

The search for new magnetoresistive materials has commanded much attention for the past few years due to the enormous variety of fascinating physical properties exhibited.¹⁻³ The need for new magnetic recording devices has provided a further impetus for the discovery of CMR and GMR materials, and an understanding of the phenomena at some fundamental level. In recent years, the perovskite LaMnO_3 has been the target of extensive doping, usually by “hole” doping, i.e., substituting the La^{3+} ion by M^{2+} ions such as Ca, Sr, Ba, or Pb. The $\text{La}_{1-x}M_x\text{MnO}_3$ system has been studied extensively, and has been found to exhibit a wide range of magnetic structures, and varying levels of magnetoresistance (MR) effects depending on the dopant concentration.⁴⁻⁶ The interplay between magnetic, charge, and orbital ordering in particular has been the target of intense activity leading to the discovery of a rich and varied set of phase diagrams of these materials in different doping regimes.

In contrast, the system $\text{CaMnO}_{3-\delta}$ offers another route to explore the mechanisms of magnetoresistance by providing a means to control the electron doping levels rather than the hole concentrations.⁷ The $\text{CaMnO}_{3-\delta}$ system has been studied for stoichiometric concentrations (such as $\delta=0$ and $\delta=0.5$)⁸ but it has been only recently that other compounds in this series have been revisited. Previous electron diffraction experiments have revealed the existence of possible oxygen vacancy ordering for commensurate values of $\delta(0.2, 0.25, 0.33, 0.5)$ as evidenced through observed superlattice reflections.⁹ As each oxygen vacancy creates two Mn^{3+} sites, this indicated that there should exist exchange pathways of Mn(III)-O-Mn(IV) , which could possibly lead to interesting

one-dimensional properties in these materials.¹⁰

The demonstration of magnetoresistance in the $\text{CaMnO}_{3-\delta}$ system which is heavily dependant on the oxygen vacancy concentration has rekindled interest in this material, and the connection with magnetic double exchange interactions and possible CMR.⁷ Magnetic susceptibility measurements have indicated the presence of a large and negative Weiss constant and several unusual low-temperature features, which include a divergence in the field-cooled and zero-field-cooled data at about $T_N \sim 125$ K.¹⁰ This has been interpreted as an antiferromagnetic phase transition, as noted by Wollan and Koehler¹¹ in the parent compound CaMnO_3 , but as of yet no magnetic neutron scattering measurements have been made on this series of materials.

This work details a study of $\text{CaMnO}_{3-\delta}$. An understanding of the subtle ordering in these materials is crucial to a complete understanding of the magnetoresistance phenomena.

EXPERIMENTAL PROCEDURES

Powder samples of $\text{CaMnO}_{3-\delta}$ ($\delta=0.06,0.11$) were prepared by the Pechini citrate gel process.⁷ Stoichiometric quantities of $\text{Mn}(\text{NO}_3)_2$ (Aldrich, 49.7% w/w aqueous solution) and CaCO_3 (Aldrich, 99+ %) were dissolved in excess amounts of nitric acid, citric acid, and ethylene glycol. After drying, the resin was heated to 600 °C to decompose the organic impurities, and the resultant material was pressed into pellets for firing. The samples were sintered in air to 1100 °C for 24 h, and then quenched, at 1100 and 1000 °C for the $\delta=0.11$ and 0.06, respectively, to room temperature.

The products were characterized using the facilities at Rutgers University. Powder x-ray-diffraction data were ob-

TABLE I. Room-temperature lattice parameters and magnetic properties of $\text{CaMnO}_{3-\delta}$. The Néel temperatures and ordered moments are quoted from the refinements. The two values under the $\text{CaMnO}_{2.89}$ compound are for the Mn^{4+} and Mn^{3+} sites, respectively. The lattice constants for the $\text{CaMnO}_{2.89}$ impurity phase are listed for comparison.

	a	b	c	T_N	μ_{ordered}	$\mu_{\text{eff}}(\text{calc})$	$\mu_{\text{eff}}(\text{exp})$	θ_C
$\text{CaMnO}_{2.94}$	5.2729(6) Å	7.4416(6) Å	5.2554(6) Å	126.0(8) K	2.36(4) μ_B	4.44(1) μ_B	3.99 μ_B	-529(1) K
$\text{CaMnO}_{2.89}$	5.270(2) Å	7.473(2) Å	5.284(2) Å	126(2) K	2.45(20) μ_B	4.89(1) μ_B	4.10 μ_B	-450(2) K
$\text{CaMnO}_{2.89}$ impurity	5.220(2) Å	7.483(3) Å	5.325(2) Å	127(3) K	4.00(30) μ_B			

tained using a SCINTAG PAD V diffractometer with $\text{CuK}\alpha$ radiation and a silicon standard. The resultant lattice parameters were refined using a least squares minimization technique. The magnetic susceptibility from 4–400 K was measured using a SQUID magnetometer (MPMS, Quantum Design), and magnetoresistive properties were observed using a standard four-probe technique.⁷

Magnetic measurements were confirmed at McMaster University using a Quantum Design MPMS SQUID magnetometer. Field cooled (FC) and zero field cooled runs (ZFC) were completed in a temperature range of 5 to 350 K with an applied magnetic field of 0.01 T.

Neutron scattering experiments were completed on the powder samples at the Dualspec C2 beamline operated by the Neutron Program for Materials Research of the National Research Council of Canada at the Chalk River Laboratory. The wavelength of the neutrons was $\lambda = 2.37086(9)$ Å. The samples were sealed in vanadium cans in a He atmosphere with an indium wire gasket. Data were taken over a temperature range of 11 K to room temperature, covering a range in 2θ of 10° to 90° . The room temperature data sets were obtained out to $2\theta = 120^\circ$ to obtain a very accurate determination of the crystallographic unit cell. The Rietveld refinements of the datasets were completed using FULLPROF (FULL98). The $\text{CaMnO}_{2.89}$ sample was found to have two very similar crystallographic phases (one of them comprising approximately 25% of the material), which was confirmed by x-ray experiments done at McMaster using a $\text{CuK}\alpha_1$ source and a Guinier-Hägg camera with Si as an internal standard. As a result, a three-phase refinement was carried out on this material, two crystallographic and one magnetic in origin.

RESULTS

Structure of $\text{CaMnO}_{2.94}$. The crystal structure and lattice parameters of $\text{CaMnO}_{2.94}$ were consistent with the values found using x-ray diffraction at Rutgers University. $\text{CaMnO}_{2.94}$ crystallizes in an orthorhombic perovskite structure with space group Pnma (Table I). The Mn ions form a network of corner-shared octahedra, with Ca ions occupying the interstitial positions (Fig. 1). The increased size of the unit cell as oxygen defects are introduced is expected as the Mn^{3+} ion has a slightly larger radius than Mn^{4+} .¹² The oxygen defects are found from refinement to be on the shared corners of the equatorial plane of the Mn octahedra; the O2

positions of $8d$ symmetry [Table II and figure 2(a)]. The defect concentration correlates well with the titration analysis (roughly 6% oxygen defects or 12% Mn^{3+} concentration for $\text{CaMnO}_{2.94}$). Each O defect creates two Mn^{3+} sites in the lattice, which effectively provides a method for electron doping these materials, in contrast to hole doping as in the $\text{La}_{1-x}\text{Ca}_x\text{MnO}_3$ series.¹³

Structure of $\text{CaMnO}_{2.89}$. The full refinement of the $\text{CaMnO}_{2.89}$ sample proved to be much more difficult than the $\text{CaMnO}_{2.94}$ member in the series. Attempts were first made using the lattice constants and space group Pnma as reported previously.⁷ The results of these refinements were not unreasonable, but upon closer examination, it was clear that some relatively strong reflections, in particular the strong secondary peak at $2\theta \sim 66^\circ$ could not be indexed [see Fig. 2(b)]. There were also a set of weak peaks which were first thought to be due to an impurity phase.

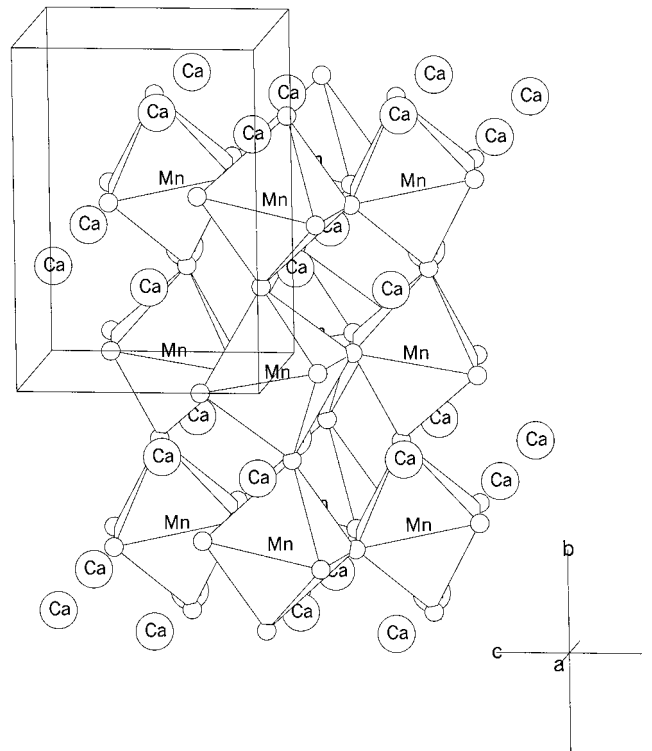


FIG. 1. The crystal structure of $\text{CaMnO}_{2.94}$.

TABLE II. Refined atomic positions and their estimated standard deviations at $T=11$ K ($\text{CaMnO}_{2.89}$) and $T=14$ K ($\text{CaMnO}_{2.94}$). The thermal parameters were refined from the $\text{CaMnO}_{2.94}$ data and left constant in the $\text{CaMnO}_{2.89}$ refinements.

$\text{CaMnO}_{2.89}$	x	y	z	Occ.
Ca	0.043(8)	0.25	-0.004(12)	1.0
Mn	0	0	0.5	1.0
O(1)	0.480(7)	0.25	-0.079(6)	1.0
O(2)	0.271(9)	0.0180(6)	-0.293(6)	0.92(4)

$\text{CaMnO}_{2.94}$	x	y	z	Occ.	B_{iso} (\AA^2)
Ca	0.033(1)	0.25	-0.013(3)	1.0	0.58(21)
Mn	0	0	0.5	1.0	0.05(27)
O(1)	0.489(1)	0.25	0.055(2)	1.0	0.42(22)
O(2)	0.288(1)	0.038(1)	-0.287(1)	0.96(2)	0.42(22)

In a first attempt to analyze the data the presence of a structurally similar impurity phase was assumed. In this doping regime, reports of impurity phases are not uncommon. For example, Chiang and Poeppelmeier found such an impurity phase in $\text{CaMnO}_{2.75}$.¹⁴ Santhosh *et al.* investigated the series of related materials $\text{Ca}_{1-x}\text{Bi}_x\text{MnO}_3$ in the regime $x \leq 0.25$, and found that for the $\text{Bi}_{0.18}\text{Ca}_{0.82}\text{MnO}_3$ compound in particular, a crystallographically similar impurity phase was present at about 29 wt. % concentration.¹⁵ Clearly, this region of the phase diagram is prone to phase separation.

Cell constants for a perovskitelike orthorhombic impurity phase were refined from powder x-ray data obtained with $\text{CuK}_{\alpha 1}$ radiation and a Guinier-Hagg camera [$a = 5.228(1)$ \AA , $b = 7.488(1)$ \AA , and $c = 5.3302(9)$ \AA at $T = 290$ K]. In the two phase refinement the atomic positions of the impurity phase were fixed to those of $\text{CaMnO}_{2.94}$ and the scale factor was varied. The concentration of the impurity phase was seen to be ~ 25 wt. % by comparison of the scale factor for the two phases. Final atomic positions for the majority phase are listed in Table IIIb. The temperature factors were found to be unstable in the refinements, and were set to the values found for $\text{CaMnO}_{2.94}$.

While the two phase approach accounts for the strong reflections in the powder pattern, several very weak reflections ($<1\%$ intensity of a strong reflection) remained unindexed (Fig. 3). Thus, an attempt was made to index these on a supercell. Again, Chiang and Poeppelmeier observed a set of weak reflections in $\text{CaMnO}_{2.75}$ which could be indexed on a $a \times b \times 4c$ supercell (Pnma setting) which they attributed to the ordering of oxygen vacancies. They were not successful, however, in refining a unique model for the vacancy ordering. Using 8–10 weak reflections of the type shown in Fig. 3, a supercell, also of dimensions $a \times b \times 4c$ (Pnma subcell setting) could be assigned to the major phase in $\text{CaMnO}_{2.89}$. As in the case of Chiang and Poeppelmeier, attempts to refine a unique model for the vacancy ordering were unsuccessful due in part to the weakness of the superlattice reflections and the complicating factor of the second phase. It is thus likely that even at room temperature there exists oxide vacancy ordering in the majority phase in $\text{CaMnO}_{2.89}$ but a detailed

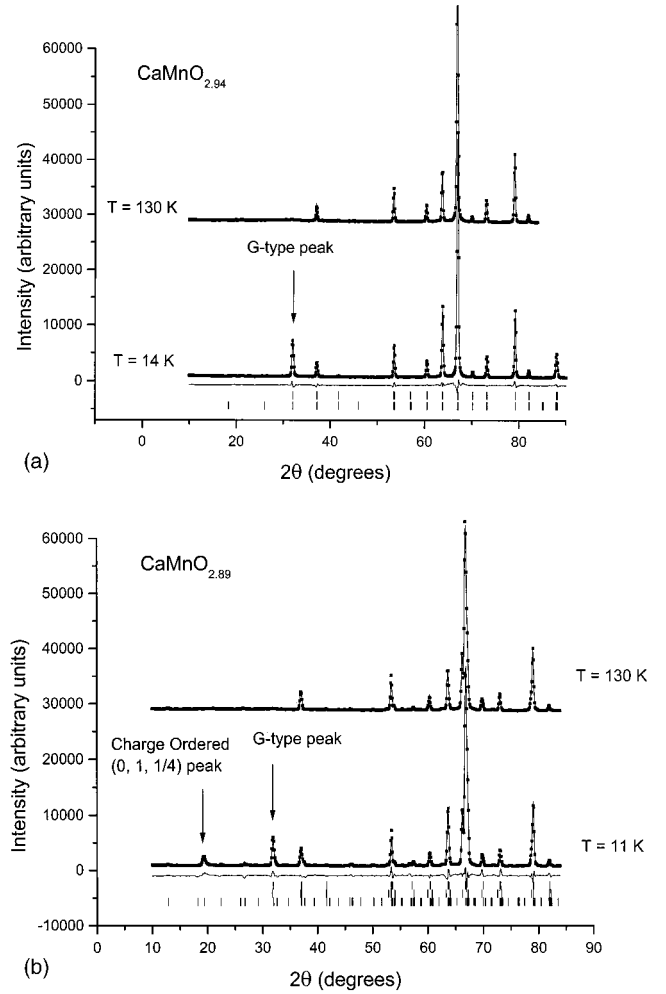


FIG. 2. (a) The neutron diffraction pattern of $\text{CaMnO}_{2.94}$ at $T = 14$ K and $T = 130$ K. The upper set of tickmarks are for the crystallographic reflections, and the lower are for the magnetic phase. (b) The neutron diffraction pattern of $\text{CaMnO}_{2.89}$ at $T = 11$ K and $T = 130$ K. The upper set of tickmarks are for the primary $\text{CaMnO}_{2.89}$ phase, the middle set are for the crystallographic impurity, and the bottom set is for the G -type+charge-ordered structures.

TABLE III. Selected interatomic distances and bond angles.

	$\text{CaMnO}_{2.94}$ ($T = 14$ K)	$\text{CaMnO}_{2.89}$ ($T = 11$ K)
Mn-O(1)	1.8840(14) $\text{\AA} \times 2$	1.9173(74) $\text{\AA} \times 2$
Mn-O(2)	1.9077(14) $\text{\AA} \times 2$	1.965(40) $\text{\AA} \times 2$
	1.8986(52) $\text{\AA} \times 2$	1.806(45) $\text{\AA} \times 2$
O(2)-Mn-O(2)	88.89(36)	89.82(79)
	91.11(39)	90.18(91)
O(1)-Mn-O(2)	87.63(38)	84.16(86)
	92.37(34)	95.84(88)
	91.75(22)	95.20(84)
	88.25(36)	85.81(80)
Mn-O(1)-Mn	161.850(64)	154.04(31)
Mn-O(2)-Mn	155.87(22)	163.28(92)

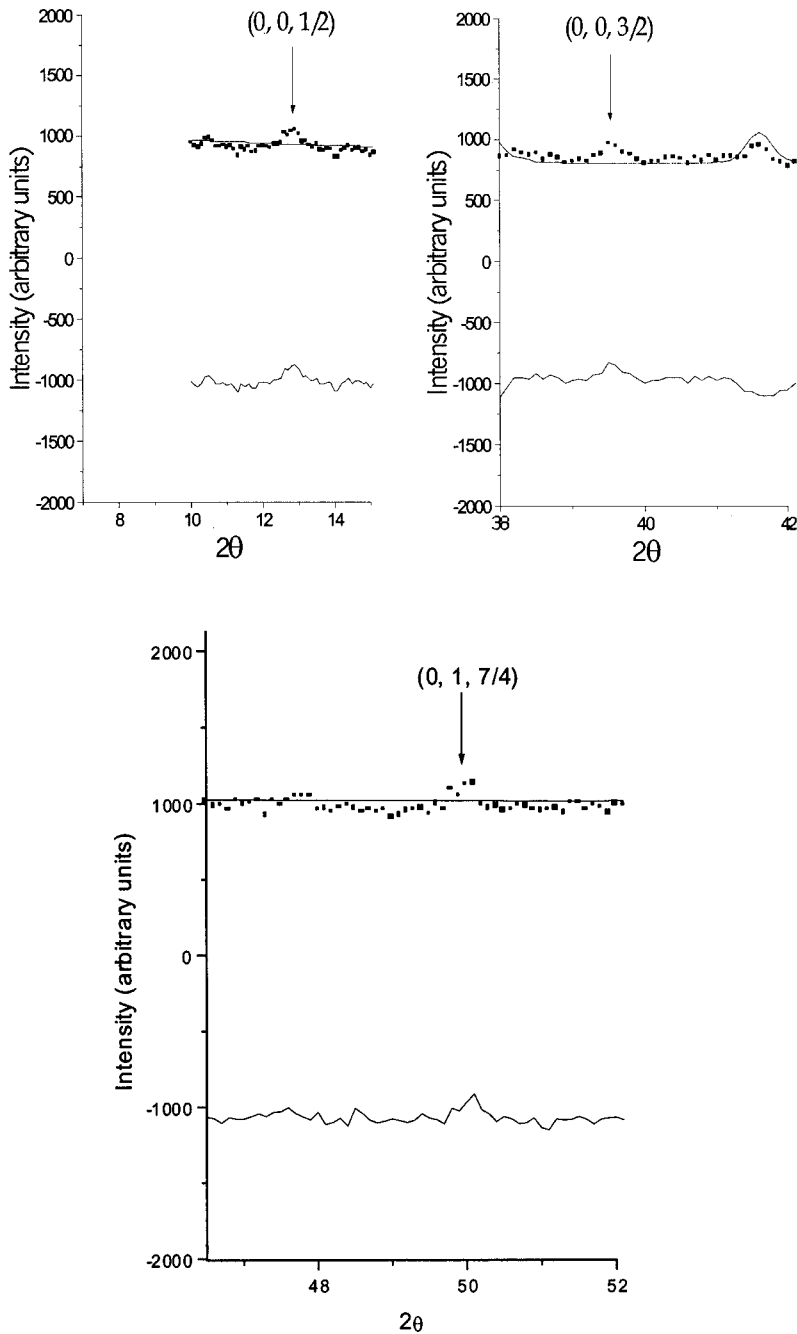


FIG. 3. Evidence of possible vacancy ordering in CaMnO_{2.89}. The superstructure peaks $(0, 0, \frac{1}{2})$, $(0, 0, \frac{3}{2})$, and $(0, 1, \frac{7}{4})$ are shown here at $T = 130$ K, which along with other weak reflections can be indexed on the cell $a \times b \times 4c$.

model is not available. Although it has been suggested that oxide vacancy ordering may induce Mn³⁺/Mn⁴⁺ charge ordering, this cannot be confirmed from the present data.

Magnetism in CaMnO_{2.94}. The magnetic structure of CaMnO₃ was among the first to be studied with neutron diffraction.¹¹ The magnetic Mn⁴⁺ sublattice consists of two interpenetrating face centred arrays of moments with antiparallel nearest neighbor spin arrangements, the so-called type *G* structure (Fig. 5). The Néel temperature is 130 K, and the effective magnetic moment is $2.43 \mu_B$, which agrees well with the spin-only value for Mn⁴⁺ ($3.00 \mu_B$).¹¹

Previous magnetic susceptibility measurements indicated a feature at 125 K which implied the possibility of long range antiferromagnetic ordering in both CaMnO_{2.94} and CaMnO_{2.89}.⁷ Our measurements confirm this in the FC/ZFC

CaMnO_{2.94} and CaMnO_{2.89} data sets (Fig. 4). The sharp cusp in the ZFC susceptibility at $T \sim 125$ K is a tell-tale sign of antiferromagnetic ordering in both materials. The values for the effective moments and the Weiss constants extracted from high-temperature Curie-Weiss fits ($T = 300 - 350$ K) agreed well with the published results, indicating a mixture of Mn³⁺ and Mn⁴⁺ moments and strong antiferromagnetic interactions.⁷ The differences between the experimental and calculated effective moments have been attributed to ferromagnetic interactions from Mn³⁺-Mn⁴⁺ clusters.¹⁰

From the neutron diffraction data, Fig. 2(a) the magnetic structure of CaMnO_{2.94} was readily identified as the *G* type found for CaMnO₃ (Fig. 5). The Rietveld refinements produced very acceptable *R* values for the crystallographic and magnetic phases ($R_p = 4.02$, $R_{wp} = 5.58$, $R_{mag} = 2.12$ at T

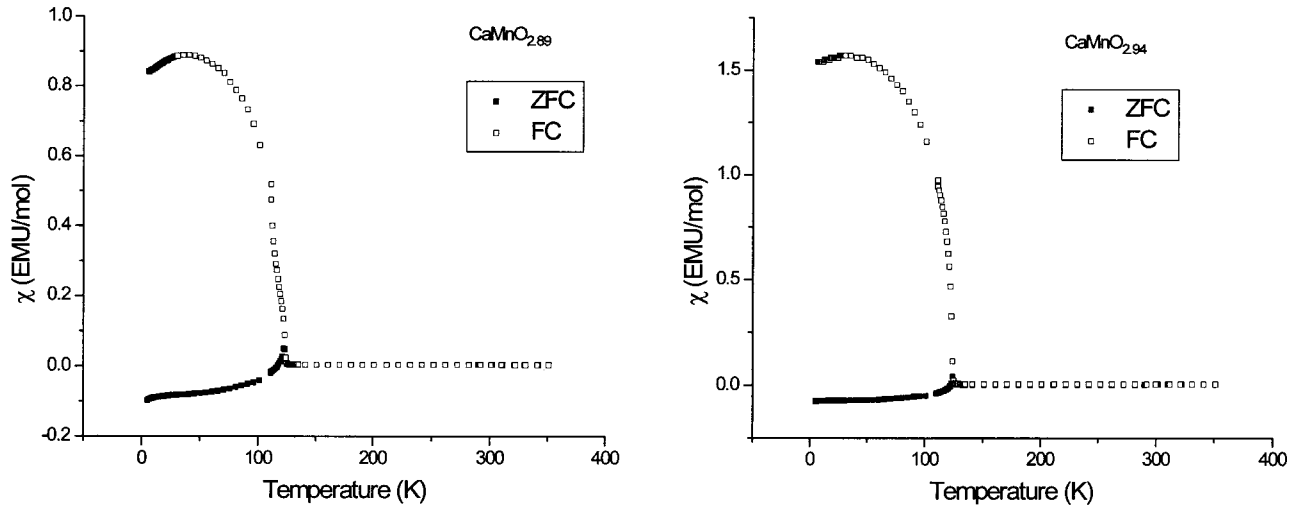


FIG. 4. The magnetic susceptibility of $\text{CaMnO}_{2.89}$ (left) and $\text{CaMnO}_{2.94}$ (right) for an applied field of $H=0.01$ T.

=14 K). The value for the ordered moment was found to be slightly smaller, $\mu=2.36(4)\mu_B$, compared to the value for CaMnO_3 of $2.43\mu_B$.¹¹ This is somewhat surprising as the average Mn moment should be larger, given that a larger spin-only moment ($4.0\mu_B$) should be associated with Mn^{3+} which comprise $\sim 12\%$ of the Mn sites.

The behavior of the ordered moment as a function of temperature is typical of three-dimensional Heisenburg-like ordering (Fig. 6). More precise measurements of the order parameter are needed to get an exact determination of the phenomena, but a guide to the eye has been drawn based upon the following scaling relationship:¹⁶

$$M(T) \sim \{(T - T_C)/T_C\}^{2\beta}.$$

The values extracted from the fit, $\beta=0.32(4)$ and $T_C=126.0(8)$ K, are consistent with $\beta=0.33$ and $T_C \sim 125$ K, as determined from the magnetic susceptibility measurements.

Magnetism in $\text{CaMnO}_{2.89}$. The magnetic Bragg peaks which appear below $T_N \sim 125$ K can be divided into two cat-

egories: the same ‘‘G-type’’ reflections as $\text{CaMnO}_{2.94}$, albeit of slightly altered intensities, and a set of reflections that can be indexed on a $(0, 0, \frac{1}{4})$ ordering wave vector [such as $(0, 1, \frac{1}{4})$, $(1, 1, \frac{1}{4})$ and $(0, 1, \frac{5}{4})$]. Since the $\text{CaMnO}_{2.89}$ sample has a higher concentration of oxygen defects, and hence a larger density of Mn^{3+} moments than $\text{CaMnO}_{2.94}$, it was hypothesized that the new Bragg peaks were due to an ordering of Mn^{3+} moments in the Mn^{4+} G-type network. The strongest new magnetic reflection in the diffraction pattern can be indexed as $(0, 1, \frac{1}{4})$. This points to an arrangement of Mn^{3+} moments that are antiferromagnetically coupled in rows along the b direction and stacked with a periodicity of four in the c -axis direction (Fig. 5). This model is appealing in that the G-type structure of CaMnO_3 and $\text{CaMnO}_{2.94}$ is preserved for low Mn^{3+} doping levels while allowing for charge-ordering at higher doping levels. The full refinement of this model for the $\text{CaMnO}_{2.89}$ dataset was complicated by a number of factors. Among them include the existence of a second crystallographic phase (comprising 25% of the sample), and a set of weak supercell reflections indicative of oxygen vacancy ordering. Several refinements were completed of the magnetic and charge ordered structures independently of one another until a suitable model was found to describe the observed diffraction pattern. Once a proper model was found, the charge and spin ordered phases were combined into one coherent model ($R_p=7.86\%$, $R_{wp}=10.71\%$, $R_{\text{mag}}=25.6\%$ at $T=11$ K).

However, the concentration of ordered Mn^{3+} ions in the model, 12.5%, is not consistent with the concentration, 22%, expected from the chemical analysis if one assumes that the electrons are completely localized on the Mn^{3+} sites. This suggests only partial charge ordering, with the residual Mn^{3+} moments distributed randomly on the lattice. Previous works have indicated that there is a significant reduction in the resistivity of this sample as compared to $\text{CaMnO}_{2.94}$,⁷ which suggests that there is an increase in the density of states at the Fermi energy even below the ordering temperature. Further transport studies are needed to resolve this problem.

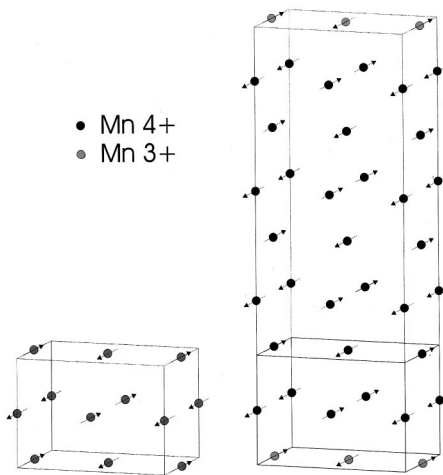


FIG. 5. The magnetic structure of $\text{CaMnO}_{2.94}$ (G-type structure, on the left) and $\text{CaMnO}_{2.89}$ (G-type charge-ordered structure).

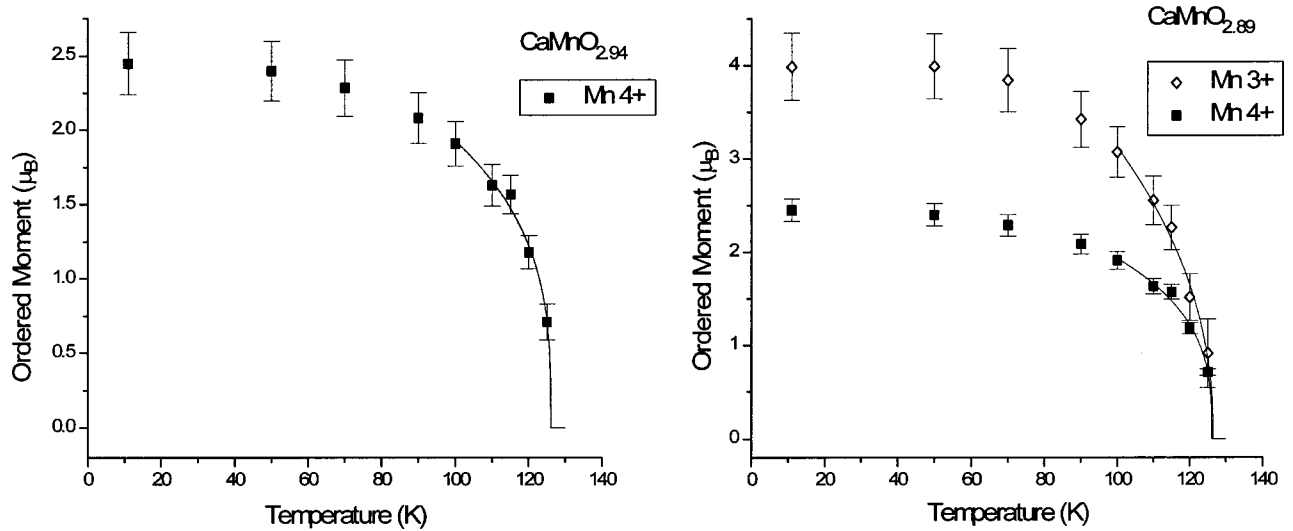


FIG. 6. The ordered moment as a function of temperature for $\text{CaMnO}_{2.94}$ (left) and $\text{CaMnO}_{2.89}$ (right) as determined from neutron scattering measurements. The fits are guides to the eye based on the power law $M(T) \sim \{(T - T_C)/T_C\}^{2\beta}$.

Although the magnetic structure described above appears to be unique for manganate perovskites, there is a recent report by Santhosh *et al.* which indicates that a weak magnetic superstructure has been reported for $\text{Bi}_{0.18}\text{Ca}_{0.82}\text{MnO}_3$ of the form $a \times b \times 4c$ but no detailed model has been proposed.¹⁵ As well, a *C*-type, not *G*-type AF order is found. There is clearly a structural analogy between the two materials, and further work is needed to understand them both.

The ordered moments for the two kinds of magnetic species seem to correlate well with the expected spin-only values for Mn^{4+} and Mn^{3+} [$2.45(20)\mu_B$ and $4.00(30)\mu_B$, respectively]. The Néel temperatures for the type *G* and $k = (0, 0, \frac{1}{4})$ components, as determined by power law fits, agree to within experimental error [126(2) K and 127(3) K, respectively, Fig. 6].

DISCUSSION

It is natural to compare and contrast the results obtained for the oxygen vacancy doped compounds $\text{CaMnO}_{3-\delta}$, with trivalent cation doped materials of similar electron doping levels (Mn^{3+} concentrations) in terms of issues such as charge-ordering and magnetic ordering, including the magnetic structure and magneto-transport properties. In fact, data on such systems are relatively sparse as most attention has been focused on the hole-doped regime, i.e., Mn^{3+} concentrations $>50\%$ where CMR effects are observed. Nonetheless, the available data on systems such as $M_{0.20}\text{Ca}_{0.80}\text{MnO}_3$, where $M = \text{La}^{3+}$ or Bi^{3+} ,¹⁷ indicate that significant differences exist.

In the case of transport behavior, the $\text{CaMnO}_{3-\delta}$ materials are much less conducting than their cation doped counterparts. As the previous study indicated,⁷ the room temperature resistivities for $\text{CaMnO}_{3-\delta}$ are in the range from 2 to 10 Ωcm even for relatively high doping levels, $\delta = 0.11$ ($\sim 22\% \text{Mn}^{3+}$) whereas the corresponding cation doped materials show values which are lower by factors of 10^2 to 10^3 , i.e., approaching (but not quite reaching) the metallic regime.

This shows either that the e_g electrons are much less mobile or that the nominal carrier density is much lower in the oxide vacancy than in the cation doped systems. Nonetheless, the observed negative magneto-resistances are of the same order of magnitude, 40–50% for both series.

Concerning the issues of charge and magnetic ordering, for the cation doped compounds anomalies in the resistivity and magnetization at temperatures above T_C for magnetic AF order have been taken as evidence of charge ordering.¹ For example, $\text{La}_{0.20}\text{Ca}_{0.80}\text{MnO}_3$ shows such anomalies at about 195 K whereas AF order sets in only below ~ 120 K.^{18,19} Similar results are found for $\text{Bi}_{0.18}\text{Ca}_{0.82}\text{MnO}_3$ where T_{CO} (charge ordering) is 210 K and $T_C(\text{AF}) = 160$ K. In sharp contrast $\text{CaMnO}_{2.94}$ and $\text{CaMnO}_{2.89}$ show only a single anomaly in the susceptibility at 125 K which corresponds to $T_C(\text{AF})$ already shown. There is no indication of a higher temperature T_{CO} up to 300 K for either material, although, as has been argued, it is difficult to understand the magnetic structure of the majority phase in $\text{CaMnO}_{2.89}$ without postulating charge ordering. One is left with (at least) two alternatives, namely, that T_{CO} and $T_C(\text{AF})$ are coincident for $\text{CaMnO}_{2.89}$ or that $T_{CO} > 300 \text{ K} > T_C(\text{AF})$. Possible support for the latter hypothesis is found in the form of the weak supercell reflections present already at 300 K which could be attributed to oxide vacancy ordering which may induce charge ordering as well by trapping Mn^{3+} centers in the vicinity of the vacancy. It should be noted that the charge ordering wave vector for $\text{Bi}_{0.18}\text{Ca}_{0.82}\text{MnO}_3$ was found to be incommensurate, while the oxide vacancy ordering wave vector appears to be commensurate, $k = (0, 0, \frac{1}{4})$. In $\text{La}_{0.20}\text{Ca}_{0.80}\text{MnO}_3$ two supercells were found from electron diffraction with “fourfold” and “23-fold” periodicities which were attributed to charge ordering.¹⁷ It is not clear at present if the “fourfold” structure is truly commensurate or if it is related to the one found in $\text{CaMnO}_{2.89}$ in the neutron diffraction data.

Finally, the basic magnetic structures are different for the

cation and oxide vacancy doped phases. The *C*-type structure is found for both $\text{La}_{0.20}\text{Ca}_{0.80}\text{MnO}_3$ and $\text{Bi}_{0.18}\text{Ca}_{0.82}\text{MnO}_3$, while the *G*-type structure of CaMnO_3 is conserved for both oxide vacancy compounds studied here. In the *C*-type structure, one has ferromagnetic chains which are coupled antiparallel to nearest neighbor chains while all near neighbor correlations are antiferromagnetic in the *G*-type structure. We note that for $\text{Bi}_{0.18}\text{Ca}_{0.82}\text{MnO}_3$, $\theta_C = 160$ K, a large positive value consistent with dominant ferromagnetic exchange, whereas, $\theta_C = -529$ K and -450 K for $\text{CaMnO}_{2.94}$ and $\text{CaMnO}_{2.89}$, respectively, which demonstrate dominant antiferromagnetic exchange.

Further work on these materials, especially $\text{CaMnO}_{2.89}$, should include high resolution x-ray diffraction, as for example reported recently for several members of the series, $\text{Bi}_x\text{Ca}_{1-x}\text{MnO}_3$ and $\text{La}_{0.333}\text{Ca}_{0.667}\text{MnO}_3$,²⁰ in order to establish definitively the nature of the phase separated material near $\text{CaMnO}_{2.89}$. Electron diffraction studies should be carried out to determine if the formation of stripe domains, reported recently for the cation doped systems, is also a feature of the vacancy doped materials.

CONCLUSIONS

The electron-doped MR materials $\text{CaMnO}_{2.94}$ and $\text{CaMnO}_{2.89}$ have been investigated using powder neutron dif-

fraction. The $\text{CaMnO}_{2.94}$ structure orders in the *G*-type AF structure as reported by Wollan and Koehler, but the $\text{CaMnO}_{2.89}$ exhibits charge ordering of the $\text{Mn}^{3+}/\text{Mn}^{4+}$ moments in a magnetic structure, $k = (0, 0, \frac{1}{4})$ that has not been reported before. The *G*-type arrangement of the moments is preserved as in $\text{CaMnO}_{2.94}$, but now there is an ordering of the Mn^{3+} moments in layers along the *c* axis. There is some evidence for an ordering of the oxygen vacancies, which has the same supercell as the magnetic/charge ordered cell, illustrating the strong interplay between the structure, electronic, and magnetic properties of these materials. A complete model of the MR mechanism in these materials is still elusive.

ACKNOWLEDGMENTS

The authors would like to express their gratitude to Ron Donaberger who assisted with the technical work involved with the neutron scattering experiments. C. R. Wiebe gratefully acknowledges support for this work from the Natural Sciences and Engineering Research Council in the form of a PGS B. This project was also supported through a research grant to J. E. Greedan through the Natural Sciences and Engineering Research Council. The work at Rutgers (M. G. and Z. Z.) was supported by Grant No. NSF-DMR-96-13106.

-
- ¹Y. Tokura and N. Nagaosa, *Science* **288**, 462 (2000).
²S. Jin, T. H. Tiefel, M. McCormack, R. A. Fastnacht, R. Ramesh, and L. H. Chen, *Science* **264**, 413 (1994).
³R. von Helmolt, J. Wecker, B. Holzapfel, L. Schultz, and K. Samwer, *Phys. Rev. Lett.* **71**, 2331 (1993).
⁴Q. Huang, J. W. Lynn, R. W. Erwin, A. Santoro, D. C. Dender, V. N. Smolyaninova, K. Ghosh, and R. L. Greene, *Phys. Rev. B* **61**, 8895 (2000).
⁵P. M. Levy, *Science* **256**, 972 (1992).
⁶P. Schiffer, A. P. Ramirez, W. Bao, and S.-W. Cheong, *Phys. Rev. Lett.* **75**, 3336 (1995).
⁷Z. Zeng, M. Greenblatt, and M. Croft, *Phys. Rev. B* **59**, 8784 (1999).
⁸K. R. Poeppelmeier, M. E. Leonowicz, J. C. Scanlon, J. M. Longo, and W. B. Yelon, *J. Solid State Chem.* **45**, 71 (1982).
⁹A. Reller, J. M. Thomas, D. A. Jefferson, and M. K. Uppal, *Proc. R. Soc. London, Ser. A* **394**, 223 (1984).
¹⁰J. Briátco, B. Alascio, R. Allub, A. Butera, A. Caneiro, M. T. Causa, and M. Tovar, *Phys. Rev. B* **53**, 14 020 (1996).
¹¹E. O. Wollan and W. C. Koehler, *Phys. Rev.* **100**, 545 (1955).
¹²R. D. Shannon, *Acta Crystallogr., Sect. A: Cryst. Phys., Diffr., Theor. Gen. Crystallogr.* **32**, 751 (1976).
¹³E. Herrero, J. Alonso, J. L. Martínez, M. Vallet-Regí, and J. M. González-Calbet, *Chem. Mater.* **12**, 1060 (2000).
¹⁴C. C. K. Chiang and K. R. Poeppelmeier, *Mater. Lett.* **12**, 102 (1991).
¹⁵P. N. Santhosh, J. Goldberger, P. M. Woodward, T. Vogt, W. Lee, and A. Epstein, *Phys. Rev. B* **62**, 14 928 (2000).
¹⁶M. F. Collins, *Magnetic Critical Scattering* (Oxford, New York, 1989).
¹⁷Y. Murakami, D. Shindo, H. Chiba, M. Kikuchi, and Y. Syono, *J. Solid State Chem.* **140**, 331 (1998).
¹⁸P. N. Santhosh, A. Arulraj, P. V. Vanitha, R. S. Singh, K. Sooryanarayana, and C. N. R. Rao, *J. Phys.: Condens. Matter* **11**, L27 (1999).
¹⁹Wei Bao, J. D. Axe, C. H. Chen, and S.-W. Cheong, *Phys. Rev. Lett.* **78**, 543 (1997).
²⁰P. G. Radaelli, D. E. Cox, L. Capogna, S.-W. Cheong, and M. Marezio, *Phys. Rev. B* **59**, 14 440 (1999).